A Wireless Inductive Sensing Technology for Soft Pneumatic Actuators Using Magnetorheological Elastomers

Hongbo Wang, *Member, IEEE*, Massimo Totaro, *Member, IEEE*,
Afroditi Astreinidi Blandin, Lucia Beccai, *Member, IEEE*

***Abstract*—This paper presents a novel wireless inductive sensing technology to measure body deformation of soft pneumatic actuators (SPAs). The proposed technology exploits a magnetorheological elastomer (MRE) both as actuator's highly deformable skin and as target of the inductive sensor. When the MRE skin is deformed by internal driving and/or external load, the distance between the MRE and sensing coil changes, thereby the inductance. A flat SPA with an MRE skin is developed as a case study to validate and evaluate the proposed technology. A multiphysics finite element model is built to simulate the characteristics of the soft actuator and sensor as a single system. Experimental results highlight that this inductive sensing technology can measure the skin deformation with an effective resolution as high as 3 µm (RMS) at null deformation (50 µm at maximum deformation), without any hysteresis. Moreover, with pressure information, it is possible to retrieve both the deformation caused by internal driving and external load. A typical pneumatic bending actuator was developed to demonstrate its easy implementation in soft actuators. The presented technology does not require wires or mechanical connections between electronics and the deformable body, providing a promising sensing solution for SPAs and other soft systems.**

I. Introduction

In the last decades, soft robotics has become an emerging research field [1-3], opening new possibilities for an inherently safe robotic-enabled society. Among all types of soft actuation mechanisms, soft pneumatic actuators (SPAs) [4] have raised interest due to their design flexibility, low cost, and simple control method. Building on intrinsically soft materials, soft-bodied robots can actively and passively change their shape to perform various tasks safely and effectively. However, this beneficial feature also makes it difficult to predict the response of a soft robot accurately due to the complex behaviors of the hyperelastic materials used. Besides internal driving, external loads can also deform soft robots, causing changes in their position, shape and movement that should be perceived to facilitate control. Additionally, in order to interact with humans and the environment, and to effectively explore the unstructured world, soft robots must be able to detect external stimuli [5]. From the sensing point of view, deformations caused by internal driving and external load are the same[6], thus, discrimination between proprioception and tactile sensing is much more difficult for soft robots than for their rigid counterparts.

To be seamlessly integrated into soft robots, sensors must be compliant enough to maintain the mechanical properties of the integrated systems and the freedom of deformation of the actuators. In the last decade, numerous soft strain and pressure sensors have been developed [7] for robotics, biomedical and wearable systems. As summarized and discussed in Wang et al. [6], researchers have explored different transducer mechanisms, from resistive, piezoresistive, capacitive, piezoelectric, to optical, magnetic and inductive. In order to build these transducers in soft form, various soft conductive materials and structures [8] have been exploited, including liquid metal, ionic liquid/hydrogel, conductive polymers and hydrogels, nanocomposites, conductive textile, wrinkling films and serpentine wires/ribbons etc. Liquid metal-based resistive sensors [9] have become a popular solution for soft robots due to the inherent high stretchability and good conductivity, while direct fabrication of micro-channels inside the actuators' soft body is difficult. Recently, stretchable waveguide optical sensors [10] have also been exploited to sense strain and pressure for SPAs, but multi-step fabrication procedures are required to embed these sensors into the actuator's body.

To date, most investigations focus on integrating soft strain sensors on the strain constrained surface of actuators to measure the bending angle, while the inflation or deformation of the soft bodies has not been directly monitored. Due to the limited stretchability of most conductive materials and structures, as well as the wiring issue [11], it is challenging to directly integrate them into highly deformable soft bodies. Recent studies demonstrated different sensing approaches in soft bodies, and highlighted the benefits of having sensory feedback. In 2016, soft hyperelastic capacitive sensors with ionic-hydrogel electrodes [12] were developed as the inflatable skins of a crawling robot to sense either the external pressure or the degree of deformation of the air chamber. In 2018, Truby et al. [13] reported a remarkable example of embedded 3D printing of ionogels-based resistive sensors for soft actuators. These notable printing technologies demonstrated full integration of soft sensors and actuators, but wire connections between the deformable body and electronics are still needed. In 2017, an optical deformation sensor was reported for SPAs, utilizing a reflective elastic diaphragm [14] to transform body deformation into light intensity. While this remote sensing technology is suitable for SPAs, a transparent or hollow optical path is essential for the

*This work has received funding from the European Union's Horizon 2020 research and innovation programme under the Marie Skłodowska-Curie grant agreement No 799773 (3D-SITS).

Hongbo Wang, Massimo Totaro, and Lucia Beccai are with the Center for Micro-BioRobotics of the Istituto Italiano di Tecnologia (IIT), Italy. Corresponding address: Viale Rinaldo Piaggio 34, 56025 Pontedera, PI, Italy; Phone: +39 050 883021. (e-mail: Hongbo.Wang@iit.it, Massimo.Totaro@iit.it, Lucia.Beccai@iit.it)

Afroditi Astreinidi Blandin is with the Center for Micro-BioRobotics of the Istituto Italiano di Tecnologia (IIT), the BioRobotics Institute of the Scuola Superiore Sant'Anna (SSSA), Pisa, Italy (e-mail: Afroditi.Astreinidi@iit.it).

optical system, which limits the flexibility of design. Alternatively, pressure or deformation can be measured remotely through magnetic field sensors, but they require an embedded rigid permanent magnet inside the deformable skin and their response can be affected by magnetic field noise [15].

To avoid stress concentration and adhesion issues, fabrication methods and materials should allow the sensing elements should be compatible with the deformable bodies of the soft robots. In particular, it would significantly ease the design and fabrication of the integrated system when the sensing mechanisms and materials originate from the actuators' body. In this paper, we present an inductive coil-based wireless sensing technology for SPAs by utilizing a highly stretchable magnetorheological elastomers (MRE), both as skin of the soft actuator and as target of the sensing system. The proposed inductive sensing technology uses part of the actuator's body to form the sensing mechanism, which provides an effortless sensing solution to directly measure the deformation of SPAs resulting from internal pressure and/or external loads. The sensor can detect a few micrometers' deformation of the actuator's skin without any hysteresis. By using the air pressure information and the inductive sensor, both the deformation caused by internal driving and the external load can be measured simultaneously. Furthermore, we demonstrate the easy implementation of this sensing technology in a bending SPA.

II. Working Principle

Inductive sensors have been widely used in industry, where two notable examples are eddy-current displacement sensors [16] and Linear Variable Differential Transformer (LVDT) position sensors [17]. In addition, inductance measurement is also a useful self-sensing approach to measure displacement, force or torque in systems involving coils and ferromagnetic materials, such as magnetorheological (MR) fluid dampers [18] and actuators [19]. Compared to (piezo-)resistive [20], optical [21], piezoelectric [22], and capacitive sensors [23], soft sensors based on inductance measurement are overlooked due to the complex fabrication of coils and the lack of integrated inductance to digital converters. In 2017, Wang et al. [24, 25] developed single and multi-axis soft inductive tactile sensors (SITS) based on the eddy-current effect, which achieved high performance and are robust enough to work in harsh environments. The SITS do not require wire connections between the sensing coil and the conductive film on the surface, providing a remote sensing solution for skin deformation and force measurement. However, the requirement of a non-stretchable conductive film still limits their applications for highly deformable SPAs. In 2018, Kawasetsu et al. presented a triaxis force sensor similar to the triaxis SITS design, using a cylindrical magnetorheological elastomer (MRE) as the sensing target instead of a conductive film [26]. The MRE is a solid composite material that consists of polymeric matrix with embedded micro- or nano-sized ferromagnetic particles, such as iron or nickel [27]. To the authors' knowledge, it is the first time that MREs are exploited to form the inductive sensing system on a SPA. As illustrated in Fig. 1, the stretchable MRE skin of the soft actuator acts as a nonconductive ferromagnetic material which can be magnetized and demagnetized at very low magnetic field, increasing the total inductance of the coil-MRE system. When the MRE skin is deformed (pressurized, under-pressurized or under external load), the average distance between MRE skin and coil changes, thereby the inductance. Therefore, the deformation of the MRE skin can be monitored wirelessly by measuring the inductance of the coil.

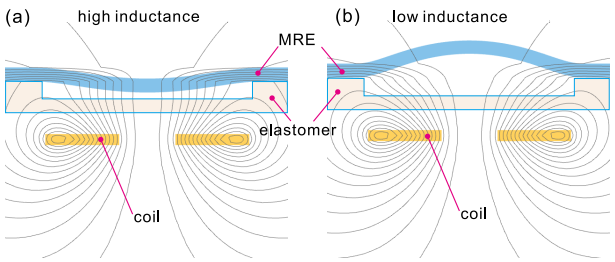

Fig. 1. Working principle of the inductive sensor for SPAs (cross section view). Magnetic field (MF) of a flat coil placed above an SPA with MRE skin (a) in a deflated state and (b) in an inflated state.

III. Prototype Development

A. SPA Design and Fabrication

To fully investigate the design parameters, characteristics and performance of the proposed sensor on SPAs, a disk-shaped flat SPA with an air chamber was designed and fabricated as a case study. The flat actuator has an outer diameter of 60 mm, and a total thickness of 6.5 mm. The thicknesses of the bottom membrane and of the top MRE skin are 2 mm. The air chamber has a height of 2.5 mm and a diameter of 30 mm. The steps of the fabrication process are depicted in Fig. 2a. To obtain the MRE skin, parts A and B of Ecoflex 0010 (Smooth-On, PA, USA) were mixed (1:1 by weight), then blended with the same weight of iron powder (Sigma Aldrich, CAS#7439-89-6, Product#12310, MO, USA), resulting 11.7% iron particles of the total composite volume. To ensure homogeneity of the particle distribution, a centrifugal mixer was used (Thinky ARE-250, CA, USA). The mixed and degassed liquid was poured into an acrylic mold and cured at room temperature. In the meanwhile, the elastomeric base was casted by mixing and curing Dragon Skin 30 (Smooth-on, PA, USA) in an acrylic mold. To assemble the two cured parts, a thin layer of liquid Dragon Skin 30 was coated on the ring-shaped top surface of the SPA

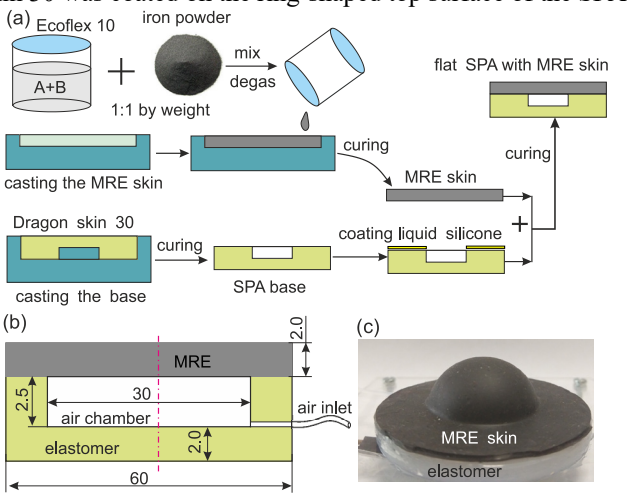

Fig. 2. (a) Fabrication procedure for the SPA with MRE skin; (b) Dimension of the SPA design (units in mm); (c) A photograph of the pressurized SPA.

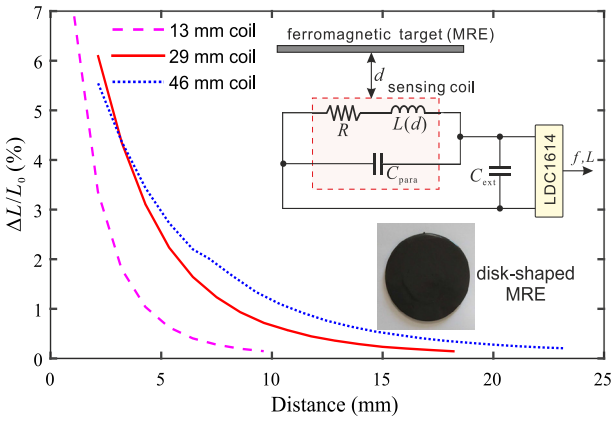

Fig. 3. Normalized inductance variation against distance between MRE and coils of different sizes, with the equivalent circuit of the inductive sensor (top right inset) and a photo of the disk-shaped MRE (bottom right inset).

base, then the MRE skin was positioned on top of it. Once this thin silicone layer is cured, the two parts are bonded together to form the air chamber. The soft flat actuator was glued to an acrylic sheet (2 mm thick) with silicone adhesive (Sil-Poxy, Smooth-On) for further testing, as shown in Fig. 2c.

B. Sensing Electronics and Coil Size

As described in [18], the inductance measurement circuit is based on a LC oscillator (the inductive coil and an external capacitor connected in parallel), as shown in the inset of Fig. 3. An evaluation module of the inductance-to-digital converter chip LDC1614 (Texas Instruments, TX, USA) is used to measure the inductance of sensing coils with an external capacitor connected in parallel. The effective sensing range of the coil-based sensor is determined by the outer diameter of the planar coil [28]. Three PCB planar coils with an outer diameter of 13 mm, 29 mm, and 46 mm (coil M, J, and H of the Reference Coil Board, LDCCOILEVM, Texas Instruments, TX, USA) were used to test how the coil size affects the sensitivity and the sensing range. A disk-shaped MRE was fabricated with the process and ratio described in section III. A., with a thickness of 2.5 mm and a diameter of 60 mm. Then, this MRE was placed above the three coils respectively at an increasing distance, while the corresponding inductance was recorded. As shown in Fig. 3, the smaller the coil diameter, the higher the sensitivity, but the narrower the sensing range. The dimensions of the SPA result in a distance of 6.5 mm between the bottom surfaces of the MRE skin and of the rigid base. Thus, the sensing range of the 13 mm coil is too small to measure the deformation of the inflated MRE skin. Since the 49 mm coil has the lowest sensitivity, the 29 mm coil was selected for this SPA. The 29 mm coil has double-layer spiral loops with 35 turns for each layer, and a self-inductance of 82.15 μH (including 15 cm leading wires). The trace of the coil has a width of 0.1 mm and a thickness of 0.035 mm, with 0.1 mm space between loops. When the coil was placed underneath the acrylic base of the SPA, the total inductance increased to 83.56 μH due to the presence of the MRE skin. In the signal conditioning electronics, a 220 pF capacitor was connected in parallel to the coil to form an oscillator at a frequency of 1.1 MHz. The root mean square (RMS) noise of inductance measurement system is 3.5×10^{-4} μH at 100 Hz sampling rate, which provides a high resolution and large dynamic range even though the inductance variation is relatively small compared to resistive sensors.

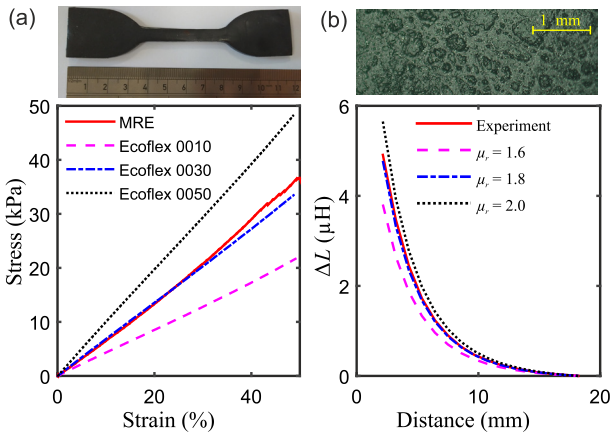

Fig. 4. Characteristics of the MRE material (a) Tensile test results of the MRE compared to Ecoflex elastomers, with (top) a photo of a testing sample; (b) Inductance variation of a planar coil-MRE disk pair against the distance between them and (top) a magnified view of the MRE skin surface. Different values are considered for the relative magnetic permeability μ_r in the FE model.

C. MRE Characterization

The mechanical properties of the MRE material (Ecoflex 0010:Iron, 1:1 by weight) were tested using a Zwick/Roell Z005 materials testing machine (Ulm, Germany), under the tension test standard for vulcanized rubber and thermoplastic elastomers (ASTM-D412 15a). All experiments were conducted on three samples and repeated 10 times. Fig. 4a shows the stress-strain curve of one loading of a sample. While the Ecoflex 0010 matrix has a Young's modulus of 45 kPa, the MRE material has an augmented stiffness provided by the iron particles, displaying a Young's modulus of 72 kPa. Up to 30% strain, the corresponding stress-strain curve almost overlaps with the one of Ecoflex 0030, which has a Young's modulus of 57 kPa. Above a strain of 30%, the MRE lies between Ecoflex 0030 and Ecoflex 0050, which has a Young's modulus of 103 kPa.

To estimate the ferromagnetic properties of the MRE materials, a finite element (FE) model was built to calculate the inductance variation of the coil-MRE pair with different of relative magnetic permeability (μ_r) values of the MRE material. The 29 mm coil and the disk-shaped MRE described in section III. B. were modeled to compare the results with the experimental data (Fig. 3). As shown in Fig. 4b, the experimental result almost overlaps with the FE model when $\mu_r = 1.8$. Therefore, we consider that the MRE has a relative magnetic permeability of 1.8, which is very low compared to bulk ferromagnetic materials (e.g. 1000 for iron). The relative permeability of the MRE can be improved by increasing the volume ratio of iron particles in the composite, but doing so will stiffen the MRE material and increase the viscosity of the uncured composite.

IV. FE Modeling and Results

Unlike for resistive and capacitive sensors, it is almost impossible to do a rigorous mathematical derivation for our inductive sensing system, as calculation of self and mutual inductances is extremely complex [29]. Simplified model [30] is useful to predict some characteristics, but would still be difficult in this case since hyperelastic materials are involved. Therefore, FE analysis was performed to investigate the characteristics of the proposed device (COMSOL®

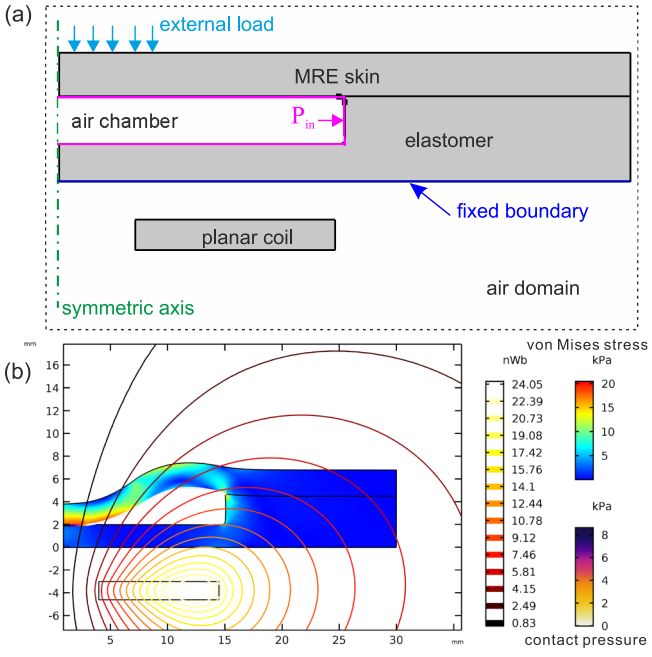

Fig. 5. (a) 2D axisymmetric geometry of the inductive sensor with the SPA for the FE model; (b) The magnetic flux (15 intensity levels) of the system and the deformed MRE skin, with von Mises stress and contact pressure shown in color scales, when both internal pressure and external load are applied.

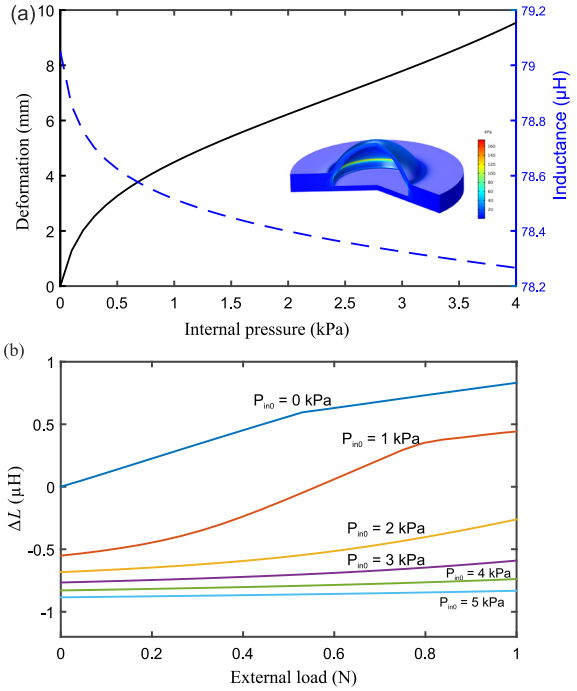

Fig. 6. FE modeling results. (a) MRE skin deformation and inductance variation of the SPA when the internal pressure of the air chamber increases from 0 to 4 kPa; (b) Inductance variations caused by external load at different initial internal pressures of the enclosed air chamber.

Multiphysics 5.3a). Both mechanics and magnetic field studies were conducted to investigate the behavior of the SPA and the sensor's response. To this aim, nonlinear solid mechanics and magnetic fields simulations have been coupled through moving mesh interface. After the solid mechanics study, the deformed geometry was imported in the magnetic field study by using the deformed mesh feature.

Exploiting the circular symmetry of the proposed device, a 2D axisymmetric model (Fig. 5a) was built for the simulation with the design and dimensions reported in Section III. A. Firstly, mechanics study was conducted with hyperelastic material models for both the MRE skin and the elastomeric base. In this case, bulk modulus $K = E/(3\times(1-2\nu))$ and shear modulus $G = E/2(1+\nu)$ were used for the Neo-Hookean hyperelastic model, where E and ν are Young's modulus and Poisson ratio, respectively. For the Poisson's ratio, 0.49 was used for both materials, and a Young's modulus of 1 MPa for the Dragon Skin 30 base, while 72 kPa for the MRE material (determined experimentally in section III. C.). Internal pressure is applied to the inner surface of the air chamber, while external load is applied to the central area of the MRE skin on its top surface. Since the external load deforms the MRE skin toward the base, mechanical contact pairs between the MRE skin and the silicone base was created in the FE model for contact calculation. Fig. 5b shows the deformation, von Mises stress and contact pressure of the SPA when both an internal pressure and a large external load are applied. In the magnetic field study, a coil with parameters described in section III. B. for the prototype is placed underneath the SPA at a distance of 2 mm to its bottom surface. A homogenized multi-turn coil feature was assigned to the coil domain to define the planar coil's parameters. A relative permeability (μ_r) of 1.8 (determined in section III. C.) and zero conductivity were used to define the electromagnetic properties of the MRE skin. The magnetic flux lines are depicted in Fig. 5b with 15 intensity levels. The total inductance of the coil-MRE system can be extracted as a global evaluation value in the AC/DC module of COMSOL.

First, an internal pressure up to 4 kPa (with a step of 100 Pa) was applied to calculate the deformation of the actuator's skin and inductance variations caused by the MRE skin's deformation. Fig. 6a indicates that the skin is deformed by 9.5 mm at 4 kPa internal pressure, while the inductance is reduced by 0.8 μH. To further investigate the sensorized SPA's response to external load, a pressure load up to 6 kPa (equals to 1.06 N total force) was applied to the actuator's upper surface at different initial internal pressures (P_{in0}) of the closed chamber. Considering that the pressure of the enclosed air chamber will change with external load as its volume changes when the skin is deformed, the ideal gas law is used to calculate the effective internal pressure of the deformed actuator and the corresponding value is imposed for each simulation step. Fig. 6b shows that higher P_{in0} leads to lower inductance and much smaller sensitivity to external loads. As a result of mechanical contact between the MRE skin and the actuator's base, turning points can be observed on the curves of P_{in0} at 0 and 1 kPa. Once the contact occurs, the device becomes stiffer, therefore less sensitive. Fig. 6b also indicates that the inductance decreases with internal pressure, but increases with external load. Thus, it is not possible to discriminate whether the skin deformation is caused by internal driving pressure or external load.

V. Results and Discussion

A. Experimental Setup

To evaluate the inductive sensor's response to MRE skin deformation of the SPA caused by both internal pressure and external load, a setup was built to conduct experiments. As

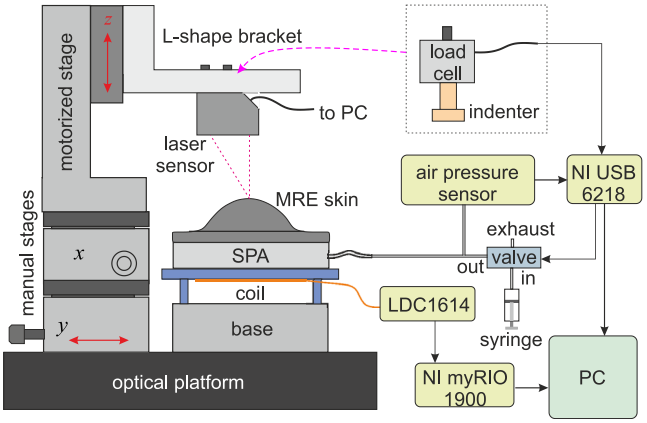

Fig. 7. Experimental setup to investigate the response of the MRE skin of the SPA to internal pressure and external load.

illustrated in Fig. 7, the manual and motorized linear stages were used to adjust the position and to apply external load. A laser displacement sensor (ILD1401-10, Micro-Epsilon, Ortenburg, Germany) was used to measure the skin deformation of the SPA. A three-port solenoid valve (V114A-5LOU, SMC Pneumatics Korea Co., Ltd., Tokyo, Japan) with a syringe was used to control the internal pressure of the SPA. In the case of applying external load, a single-axis load cell (FSH00103, FUTEK, CA, USA) with a cylindrical plastic indenter (15 mm diameter) was used to compress the MRE skin and monitor the force. A LabView-based program was developed for data acquisition and control through a NI myRIO 1900 and a NI USB 6218 (National Instruments, TX, USA).

B. Characterization of the Sensorized SPA

First, the inductive sensor was characterized to sense the deformation of the SPA under internal pressure driving. While the internal pressure of the SPA was slowly increased from -0.5 kPa (Fig. 8a) to 6 kPa (Fig. 8b), the corresponding deformation (at the central point of the circular MRE skin) and the inductance variation were recorded (Fig. 8c and Fig. 8d). As shown in Fig. 8c, the mechanical simulation results from FE modeling match well with the experiments. In contrast, the inductance variation of the prototype is smaller than the results from FE modeling, which is probably caused by mismatches between the fabricated prototype and the model. In addition, the relative permeability of the MRE skin might change when the skin is stretched, which is not considered in the FE model. To evaluate the repeatability of the sensing system, the SPA is inflated and deflated cyclically. Fig. 8e shows that there is a clear hysteresis (about 11%) between pressure and deformation, which is one of the reasons why the deformation of the SPA cannot be precisely controlled through open-loop control. Particularly, when the SPA is actuated at higher speed, aerodynamics, relaxation and nonlinear behavior of the materials will affect the real-time deformation significantly. Since the transducer mechanism directly measures the average distance between the coil and the MRE skin, this inductive sensing technology is hysteresis-free for skin deformation measurement, as shown in Fig. 8f. We can expect that the sensing system would encounter a certain level of hysteresis if the measurand is stress (or pressure, force) due to the viscoelasticity of the hyperelastic materials used. Fig. 8f also shows that the sensor's response is highly nonlinear. The curve fitting result indicates that the inductance variation to

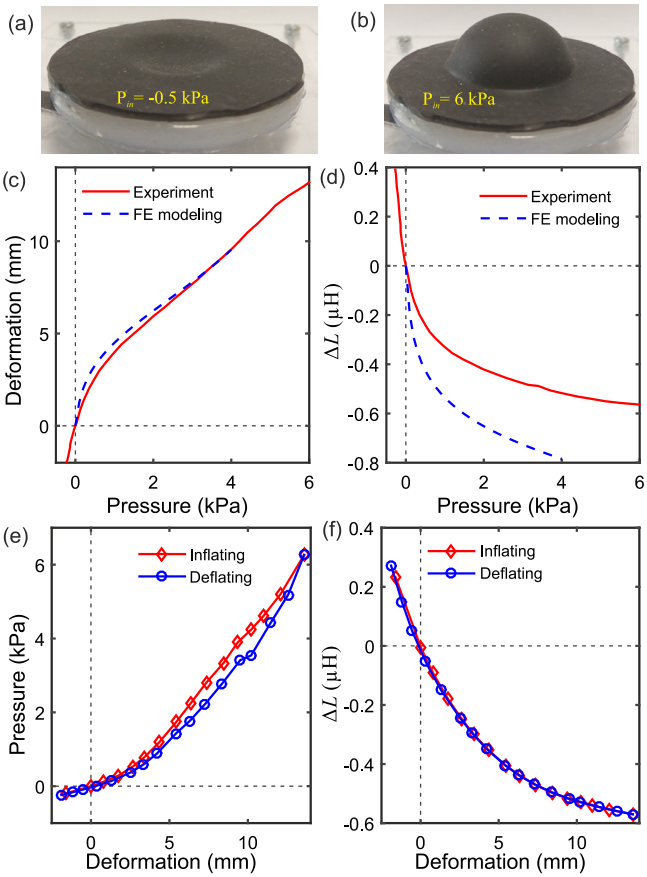

Fig. 8. Photographs of the SPA under an internal pressure of (a) -0.5 kPa and (b) 6 kPa; FE modeling and experimental characterization of the sensorized SPA under different internal pressures: (c) Skin deformation (d) Inductance variation; (e) Internal pressure against skin deformation during an inflating and deflating cycle from experiments; (f) Inductance variation during the same cycle.

deformation curve fits well with an exponential function. The sensitivity decreases rapidly from 0.12 μH/mm at 0 mm deformation to 0.007 μH /mm at 14 mm deformation. Given that the inductance measurement noise (RMS) is as low as 3.5×10^{-4} μH at 100 Hz sampling rate, the presented sensor has a very high effective resolution of 3 μm (RMS) at null deformation (50 μm at 14 mm deformation). Since the inductance was measured at a frequency around 1 MHz with a small AC current excitation, the bandwidth of electronics is more than sufficient (the maximum sampling rate is 4.08 kSPS for the LDC1614 chip). Therefore, the dynamic response is only limited by the natural frequency of the soft actuator itself.

C. Proprioception and Tactile Sensing

As discussed in the introduction, simultaneous detection of both the deformation caused by internal driving and the external load would be needed to make the soft actuator controllable and perceptive. Since air pressure sensors are frequently used in SPAs, we exploit the pressure value as a sensing information together with the inductance variation. To evaluate the idea, an external load was applied to the MRE skin of the SPA prototype with a cylindrical indenter when the air chamber of the SPA was closed by a valve connected to the inlet at a specific initial internal pressure P_{in0}. We conducted this indentation test with P_{in0} spanning from 0 to 5.5 kPa. As two examples of the test results, inductance variations and pressure changes during 5 indentation cycles for P_{in0} at 0 kPa

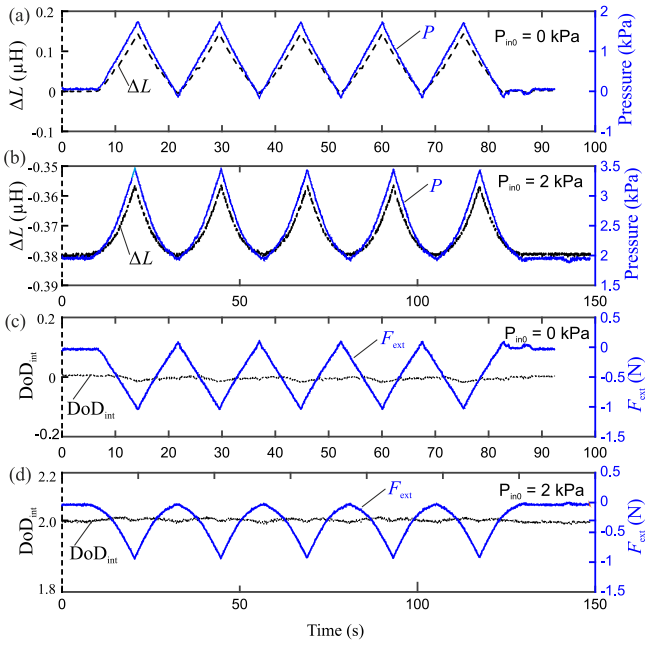

Fig. 9. Inductance variation and pressure change under cyclic external load at different initial internal pressures of the enclosed air chamber: (a) P_{in0} = 0 kPa (b) P_{in0} = 2 kPa. Both the degree of deformation and the external load are detected by combining information from the inductive and the pressure sensor: (c) P_{in0} = 0 kPa (d) P_{in0} = 2 kPa.

and 2 kPa are shown in Fig. 9a and Fig. 9b, respectively. As shown in Fig. 8c and Fig. 8d, when the SPA is inflated by increasing the internal pressure, the inductance decreases. When the air chamber is closed, external load compresses the MRE skin towards the coil, increasing the inductance; the pressure of the air chamber increases as well due to the reduced air volume. Fig. 9a and Fig. 9b highlight that the inductance and pressure vary similarly to the external load. Therefore, by combining the inductance variation and the pressure change, the degree of deformation caused by internal driving (DoD_{int}) and the external load (F_{ext}) can be discriminated by a linear combination of ΔL and P_{in}:

$$\begin{pmatrix} DoD_{int} \\ F_{ext} \end{pmatrix} = \begin{pmatrix} a_1 & a_2 & a_3 \\ b_1 & b_2 & b_3 \end{pmatrix} \begin{pmatrix} P_{in} \\ \Delta L \\ 1 \end{pmatrix} \quad (1)$$

where a_i and b_i (i=1, 2, 3) are coefficients. As shown in Fig. 9c and Fig. 9d, the DoD_{int} and the F_{ext} are decoupled. However, it should be noted that a_i and b_i are not constant for all P_{in0}. Pressure increased approximately by 1.5 kPa for both states with P_{in0} at 0 kPa and 2 kPa when 1 N external load is applied. However, the inductance variation with P_{in0} at 2 kPa is much smaller than when P_{in0} is 0 kPa since the sensitivity of the inductive sensor decays with increased distance between the MRE and the coil. Therefore, a calibration process is needed to determine the coefficients. It should be noted that given the significant hysteresis between the control pressure and the deformation caused by internal driving, it would be difficult to accurately calculate how much deformation originates from internal driving, and how much is caused by the external load. In order to achieve accurate and repeatable results, two coils should be implemented for proprioception and tactile sensing. Also, when distribution of the external loading is needed, more sensing coils should be used to detect the skin deformation at different positions.

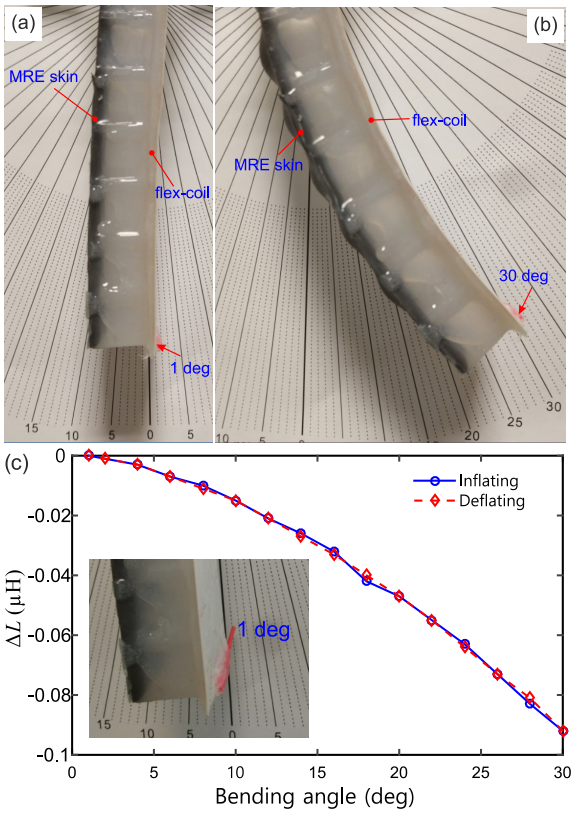

Fig. 10. Photographs of the sensorized bending SPA (a) at rest state; and (b) pressurized; (c) Inductance variation against the bending angle of the SPA during an inflation and deflation cycle; with a magnified view of the bending angle reading (inset).

D. Sensorized Soft Bending Actuator

To demonstrate its potential applications in soft robotics, we developed a soft pneumatic bending actuator with the inductive sensor. As shown in Fig. 10a, the sensorized bending actuator has a design similar to the PneuNets system [31]. In this case, the highly stretchable skin is made of MRE. A rectangular flexible coil was placed on the other side of the SPA to function as the sensing unit and also as a strain limiting layer. When no pressure is applied to the SPA, the sensor has an inductance of 36.50 μH. The inductance decreases due to the inflation of the MRE skin when the actuator is pressurized (Fig. 10b). A red needle marker was fixed at the tip (on the coil side) of the SPA to facilitate the direct reading of bending angles (inset of Fig. 10c). In this prototype, the sensor measures the average distance variations between the MRE skin and the flexible coil, which determines the bending angle of the SPA. Therefore, the bending angle measurement is hysteresis-free as well (Fig. 10c). Despite the small variation of inductance in this prototype (0.1 μH at 30°), the sensor is still able to detect less than 1° variation of the bending angle, as indicated in Fig. 10c. To improve the sensitivity and robustness, the initial distance between the MRE skin and the flexible coil should be reduced as discussed in Section III. B.

VI. Conclusion

In this manuscript, we presented a novel wireless sensing technology to measure the deformation of SPAs by utilizing stretchable MREs both as deformable skin of soft actuators and as sensing target of inductive coils. The planar coil placed underneath the SPA can directly measure the deformation of

the MRE skin through AC magnetic field coupling. A flat SPA with a single air chamber was developed to validate and evaluate this new sensing technology as a case study. Multiphysics modeling was performed to investigate both the mechanical behavior of the actuator and the corresponding response of the sensor. The inductive sensor can measure the deformation of the MRE skin with a high resolution of 50 μm (at maximum deformation) and no hysteresis during an inflation and deflation cycle. Furthermore, it is possible to detect both the deformation caused by internal driving and the external load simultaneously by also using the air pressure information. To further demonstrate this sensing technology, a typical soft pneumatic bending actuator was developed and tested, showing promising results for bending angle measurement.

The presented sensing technology has several advantages: hysteresis-free, high resolution, easy implementation, design flexibility, no additional integration process. Most importantly, it doesn't require electrical wiring or mechanical connections between the electronics and the deformable body, removing one of the key barriers in soft robotic sensing. On the other hand, it would be difficult to miniaturize the coil, leading to low spatial resolution, limiting application in micro-/nano systems, but it is promising for centimeter scale soft systems. In the near future, investigations will focus on the design and configuration of multiple coils to form a multi-modal sensing system for SPAs. Moreover, flexible planar coils can be designed and integrated in a soft robotic system (e.g. a crawling robot; or a soft gripper) for feedback control and interactions with the environment.

REFERENCES

[1] S. Bauer, S. Bauer‐Gogonea, I. Graz, M. Kaltenbrunner, C. Keplinger, and R. Schwödiauer, "25th anniversary article: a soft future: from robots and sensor skin to energy harvesters," Advanced Materials, vol. 26, pp. 149-162, 2014.

[2] C. Laschi and M. Cianchetti, "Soft robotics: new perspectives for robot bodyware and control," Frontiers in bioengineering and biotechnology, vol. 2, 2014.

[3] S. I. Rich, R. J. Wood, and C. Majidi, "Untethered soft robotics," Nature Electronics, vol. 1, p. 102, 2018.

[4] P. Polygerinos, N. Correll, S. A. Morin, B. Mosadegh, C. D. Onal, K. Petersen, et al., "Soft robotics: review of fluid-driven intrinsically soft devices; manufacturing, sensing, control, and applications in Human-Robot Interaction," Advanced Engineering Materials, 2017.

[5] L. Beccai, C. Lucarotti, M. Totaro, and M. Taghavi, "Soft Robotics Mechanosensing," in Soft Robotics: Trends, Applications and Challenges, ed: Springer, 2017, pp. 11-21.

[6] H. Wang, M. Totaro, and L. Beccai, "Toward Perceptive Soft Robots: Progress and Challenges," Advanced Science, vol. 5, 1800541, 2018.

[7] M. Amjadi, K. U. Kyung, I. Park, and M. Sitti., "Stretchable, skin-mountable, and wearable strain sensors and their potential applications: a review," Advanced Functional Materials, vol. 26, pp. 1678-1698, 2016.

[8] J. Park, I. You, S. Shin, and U. Jeong, "Material approaches to stretchable strain sensors," ChemPhysChem, vol. 16, pp. 1155-1163, 2015.

[9] E. L. White, J. C. Case, and R. K. Kramer, "Multi-mode strain and curvature sensors for soft robotic applications," Sensors and Actuators A: Physical, vol. 253, pp. 188-197, 2017.

[10] H. Zhao, K. O'Brien, S. Li, and R. F. Shepherd, "Optoelectronically innervated soft prosthetic hand via stretchable optical waveguides," Science Robotics, vol. 1, p. eaai7529, 2016.

[11] W. Dang, V. Vinciguerra, L. Lorenzelli, and R. Dahiya, "Printable stretchable interconnects," Flexible and Printed Electronics, vol. 2, p. 013003, 2017.

[12] C. Larson, B. Peele, S. Li, S. Robinson, M. Totaro, L. Beccai, et al., "Highly stretchable electroluminescent skin for optical signaling and tactile sensing," Science, vol. 351, pp. 1071-1074, 2016.

[13] R. L. Truby, M. Wehner, A. K. Grosskopf, D. M. Vogt, S. G. M. Uzel, R. J. Wood, et al., "Soft somatosensitive actuators via embedded 3D printing," Advanced Materials, vol. 30, 2018.

[14] A. M. Hart, L. O. Tiziani, J. H. Jung, and F. L. Hammond, "Deformable reflective diaphragm sensors for control of soft pneumatically actuated devices," in 2018 IEEE International Conference on Soft Robotics (RoboSoft), 2018, pp. 132-139.

[15] H. Wang, G. de Boer, J. Kow, A. Alazmani, M. Ghajari, R. Hewson, et al., "Design methodology for magnetic field-based soft tri-axis tactile sensors," Sensors, vol. 16, p. 1356, 2016.

[16] H. Wang, and Z. Feng, "Ultrastable and highly sensitive eddy current displacement sensor using self-temperature compensation," Sensors and Actuators A: Physical, vol. 203, pp. 362-368, 2013.

[17] A. Danisi, A. Masi, R. Losito, and Y. Perriard, "Electromagnetic analysis and validation of an ironless inductive position sensor," IEEE Transactions on Instrumentation and Measurement, vol. 62, pp. 1267-1275, 2013.

[18] K. H. Lam, Z. H. Chen, Y. Q. Ni, and H. L. W. Chan, "A magnetorheological damper capable of force and displacement sensing." Sensors and Actuators A: Physical, vol. 158, pp. 51-59, 2010.

[19] C. Rossa, L. Eck, A. Micaelli, and J. Lozada, "On a novel torque detection technique for magnetorheological actuators," IEEE Sensors Journal, vol. 14, pp.1223-1231, 2014.

[20] K. Kure, T. Kanda, K. Suzumori, and S. Wakimoto, "Flexible displacement sensor using injected conductive paste," Sensors and Actuators, A: Physical, vol. 143, pp. 272-278, 2008.

[21] M. Totaro, A. Mondini, A. Bellacicca, P. Milani, and L. Beccai, "Integrated simultaneous detection of tactile and bending cues for soft robotics," Soft robotics, vol. 4, pp. 400-410, 2017.

[22] Z. H. Liu, C. T. Pan, C. Y. Su, L. W. Lin, Y. J. Chen, and J. S. Tsai, "A flexible sensing device based on a PVDF/MWCNT composite nanofiber array with an interdigital electrode," Sensors and Actuators A: Physical, vol. 211, pp. 78-88, 2014.

[23] L. Viry, A. Levi, M. Totaro, A. Mondini, V. Mattoli, B. Mazzolai, et al., "Flexible three-axial force sensor for soft and highly sensitive artificial touch," Advanced materials, vol. 26, pp. 2659-2664, 2014.

[24] H. Wang, J. Kow, N. Raske, G. de Boer, M. Ghajari, R. Hewson, et al., "Robust and high-performance soft inductive tactile sensors based on the Eddy-current effect," Sensors and Actuators A: Physical, vol. 271, pp. 44-52, 2018.

[25] H. Wang, D. Jones, G. de Boer, J. Kow, L. Beccai, A. Alazmani, et al., "Design and characterization of tri-axis soft inductive tactile sensors," IEEE Sensors Journal, 2018.

[26] T. Kawasetsu, T. Horii, H. Ishihara, and M. Asada, "Flexible tri-axis tactile sensor using spiral inductor and magnetorheological elastomer," IEEE Sensors Journal, vol. 18, pp. 5834-5841, 2018.

[27] P. Song, Z. J. Peng, Y. L. Yue, H. Zhang, Z. Zhang, and Y. C. Fan, "Mechanical properties of silicone composites reinforced with micron- and nano-sized magnetic particles," Express Polymer Letters, vol. 7, pp. 546-553, 2013.

[28] H. Wang, W. Li, and Z. Feng, "A compact and high-performance eddy-current sensor based on meander-spiral coil," IEEE Transactions on Magnetics, vol. 51, pp. 1-6, 2015.

[29] W. G. Hurley, and M. C. Duffy, "Calculation of self and mutual impedances in planar magnetic structures," IEEE Transactions on Magnetics, vol. 31, pp. 2416-2422, 1995.

[30] H. Wang, W. Li, and Z. Feng, "Noncontact thickness measurement of metal films using eddy-current sensors immune to distance variation," IEEE Transactions on Instrumentation and Measurement, vol. 64, pp.2557-2564, 2015.

[31] F. Ilievski, A. D. Mazzeo, R. F. Shepherd, X. Chen, and G. W. Whitesides, "Soft robotics for chemists,", Angewandte Chemie, vol. 123, pp.1930-1935, 2011